Lawrence Berkeley National Laboratory

Title

Dispersion kinks from electronic correlations in an unconventional iron-based superconductor

Permalink

Journal

ISSN

Authors

Chang, M-H

Backes, S

Lu, D

et al.

Publication Date

DOI

Dispersion kinks from electronic correlations in an unconventional iron-based superconductor

M.-H. Chang[1,8], S. Backes[2,8], D. Lu[3], N. Gauthier[4], M. Hashimoto[3], G.-Y. Chen[5], H.-H. Wen[5], S.-K. Mo[6], R. Valentí[7] ✉ & H. Pfau[1] ✉

The attractive interaction in conventional BCS superconductors is provided by a bosonic mode. However, the pairing glue of most unconventional superconductors is unknown. The effect of electron-boson coupling is therefore extensively studied in these materials. A key signature is dispersion kinks that can be observed in the spectral function as abrupt changes in velocity and lifetime of quasiparticles. Here, we show the existence of two kinks in the unconventional iron-based superconductor $RbFe_2As_2$ using angle-resolved photoemission spectroscopy (ARPES) and dynamical mean field theory (DMFT). In addition, we observe the formation of a Hubbard band multiplet due to the combination of Coulomb interaction and Hund's rule coupling in this multiorbital system. We demonstrate that the two dispersion kinks are a consequence of these strong many-body interactions. This interpretation is in line with a growing number of theoretical predictions for kinks in various general models of correlated materials. Our results provide a unifying link between iron-based superconductors and different classes of correlated, unconventional superconductors such as cuprates and heavy-fermion materials.

Unconventional and high-temperature superconductivity almost exclusively appears in materials with strong electronic correlations. In order to determine if and to what extent correlations are a prerequisite, it is crucial to determine their effect on the electronic structure in the normal state out of which superconductivity emerges.

Abrupt changes in the electron dispersion, called "kinks", are believed to hold important clues. Kinks can appear when electronic excitations couple to collective modes such as phonons, which suggests that they also act as the superconducting pairing mechanism. Therefore, the study of dispersion kinks attracted a tremendous amount of research in the past, and many kinks have been observed experimentally[1–10]. However, their origin often remains controversial. In the context of correlated metals, it was predicted that strong interactions between electrons themselves can induce two kinks[11]. It is a feature in models of various strongly correlated systems[12–18], but observing both kinks experimentally has been challenging.

The spectral function of strongly correlated materials splits into two components: a coherent quasiparticle peak close to the Fermi energy E_F and an incoherent part forming Hubbard bands at high energies. A kink separates the coherent from the incoherent part. Such kinks have been observed in the cuprates[19–24] and ruthenates[3] in the

[1]Department of Physics, The Pennsylvania State University, University Park, PA, USA. [2]RIKEN iTHEMS, Wako, Saitama 351-0198, Japan; Center for Emergent Matter Science, RIKEN, Wako, Saitama, Japan. [3]Stanford Synchrotron Radiation Lightsource, SLAC National Accelerator Laboratory, Menlo Park, CA, USA. [4]Institut National de la Recherche Scientifique - Energie Matériaux Télécommunications, Varennes, Canada. [5]Center for Superconducting Physics and Materials, National Laboratory of Solid State Microstructures and Department of Physics, Nanjing University, Nanjing, China. [6]Advanced Light Source, Lawrence Berkeley National Laboratory, Berkeley, CA, USA. [7]Institut für Theoretische Physik, Goethe-Universität Frankfurt, Max-von-Laue-Str. 1, Frankfurt am Main, Germany. [8]These authors contributed equally: M.-H. Chang, S. Backes. ✉e-mail: valenti@itp.uni-frankfurt.de; heike.pfau@psu.edu

energy range between 300 meV and 600 meV. They are a direct fingerprint of strong electronic correlations[25–29].

The models in ref. 11–18 also predict a second kink that appears at low energies inside the quasiparticle band. The existence of this kink is less clear in other studies of the single-band Hubbard model[25,26,29]. The low-energy kink strongly renormalizes exactly those electronic excitations that condense into Cooper pairs in the superconducting state. Fermi liquid behavior only emerges below the kink energy[11,13–15]. The kink has been suggested to be accompanied by the appearance of a collective spin excitation of similar energy[12], which may be responsible for the superconducting pairing. A plethora of low energy kinks at a few tens of meV has experimentally been observed in unconventional superconductors such as cuprates[1,2], ruthenates[4], and iron-based superconductors[5–9]. However, their origin is often debated because they have an energy within the phonon as well as spin excitation spectrum. Only a few kinks could clearly be associated with electronic correlations[4,10].

Here, we study the unconventional iron-based superconductor RbFe$_2$As$_2$ with a combination of angle-resolved photoemission spectroscopy (ARPES) and fully charge self-consistent Density Functional Theory + dynamical mean-field theory (DFT+DMFT) calculations. We show that the strong electronic correlations in RbFe$_2$As$_2$ separate the spectral function into a quasiparticle peak and a multiplet of Hubbard bands, which is the prerequisite for correlation-induced kinks. Indeed, we identify a low and a high-energy kink in ARPES and DMFT and argue that both originate from strong electronic correlations. RbFe$_2$As$_2$ can, therefore, serve as a prototype material for the physics of correlation-induced kinks, and it provides a unifying link between the various classes of strongly correlated, unconventional superconductors such as cuprates, heavy fermions, nickelates, ruthenates, and iron-based superconductors.

Results

RbFe$_2$As$_2$ is a hole-doped, iron-based superconductor with a large Sommerfeld coefficient of 127 mJ/mol/K^2 [30,31], large effective masses up to 25 times the bare electron mass[32], and low coherence and Fermi liquid temperatures below 100 K[30,33–35]. These thermodynamic and transport measurements place RbFe$_2$As$_2$ among the strongest correlated iron-based superconductors. A combination of Coulomb interaction and Hund's rule coupling is responsible for the correlated nature[36–41].

The effect of correlations in the electronic structure of iron-based superconductors is most often described by renormalization factors that reduce the bandwidth of the itinerant quasiparticles[42]. At the same time, one expects a transfer of spectral weight from the coherent quasiparticle peak to the incoherent part of the spectrum. Therefore, we probe the electron-removal spectral function with ARPES across a large energy window down to 6 eV as shown in Fig. 1a. The ARPES spectrum was taken with a photon energy of 60 eV, which probes a momentum close to $k_z = 0$[43]. The chosen light polarization predominantly leads to photoemission of electrons with d_{xz} and p_x orbital character along k_x. While the photon energy dependence of their relative photoemission cross sections is rather complex, energies beyond 50 eV generally emphasize d_{xz} spectral weight[44–47] (see "methods" section for further experimental details). The ARPES spectrum shows momentum-dependent incoherent spectral weight below −0.5 eV. To highlight its energy dependence, we plot an energy distribution curve (EDC) close to the Brillouin zone center in Fig. 1b. It shows a 3-peak structure (dots) that is energetically clearly separated from the sharp quasiparticle peak at low binding energies.

Dynamical mean field theory combined with density functional theory calculations (DFT + DMFT) has proven to be a powerful method to describe and capture the correlated nature of metals such as iron-based superconductors[36,48–51]. We therefore compare our ARPES results with the theoretical spectral function obtained from a DFT+DMFT calculation, projected onto the d_{xz} orbital character, shown in Fig. 1c. We used established interaction parameters of $U_{avg} = 4$ eV, $J_{avg} = 0.8$ eV, representative for the iron-based pnictides[52,53] (see "method" section for further computational details). The EDC in Fig. 1d shows the same three-peak structure (dots) of the incoherent spectral weight. Peak positions and relative intensities match the experimental observations. The region between −2 eV and −5 eV overlaps with the expected As 4p bands and simple p-d hybridization may be responsible. However, the peak around −1 eV is absent in DFT calculations (see Supplementary Note 1 Supplementary Material).

A simple atomic model of five degenerate orbitals provides an intuitive understanding for the energy distribution of the incoherent spectral weight. In RbFe$_2$As$_2$, nominally 5.5 electrons occupy the 10 Fe 3d states. However, a statistical analysis of the DFT+DMFT orbital configurations reveals that the average occupation is in fact close to 6 electrons. The ground state can therefore be approximated as a d^6, $S = \pm 4/2$ high spin configuration due to Hund's rule coupling[40]. The three possible electron removal states, which represent Hubbard bands, are depicted in Fig. 1e. Their energies were calculated using the same interaction
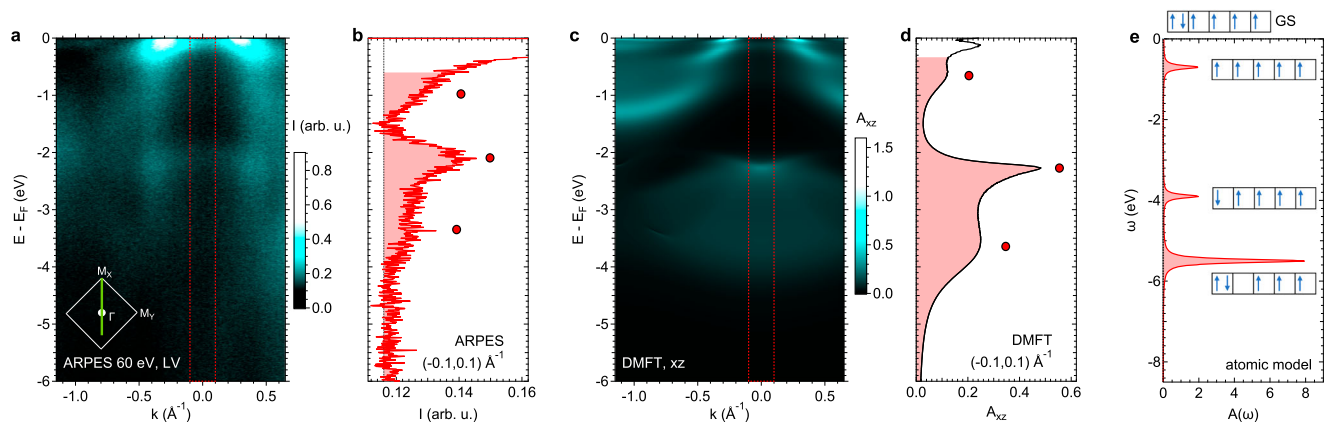

Fig. 1 | Hubbard bands in RbFe$_2$As$_2$. a ARPES spectrum taken with 60 eV, linear vertically (LV) polarized light and measured over a large binding energy window up to 6 eV. The inset shows the momentum cut (green line) through the Brillouin zone (white square). **b** EDC extracted from the ARPES spectrum integrated over a momentum window of (-0.1,0.1) Å (red dashed boxes), highlighting the incoherent spectral weight at high binding energy. **c** DMFT spectral function projected onto the d_{xz} orbital in the same energy and momentum range as the ARPES data in (**a**). **d** EDC extracted from **c** integrated over the same momentum window as (**b**). Red dots in (**b**, **d**) mark the three peaks discussed in the main text. **e** Spectrum of electron removal states in an atomic model of five degenerate orbitals. Energy levels are broadened with a Gaussian for better visibility. The electronic configuration of the ground state (GS) is shown above the plot.
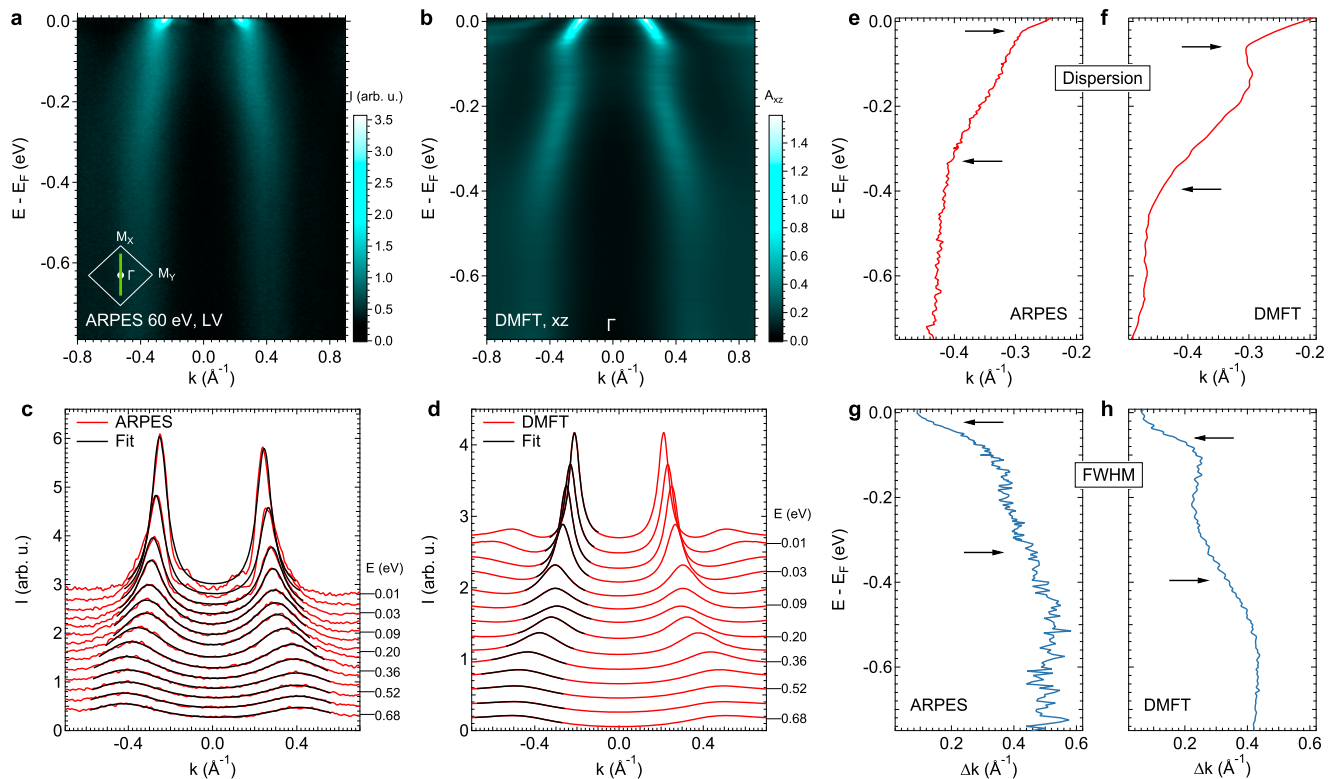
Fig. 2 | Spectral function of RbFe$_2$As$_2$. a ARPES spectrum across the Brillouin zone center taken at 20 K with a photon energy of 60 eV. We use linear vertically (LV) polarized light, which highlights the d_{xz} orbital. The spectrum was divided by a Fermi-Dirac function. Inset shows the momentum cut (green line) through the Brillouin zone (white square). **b** Spectral function along k_x calculated by DMFT and projected onto the d_{xz} orbital. **c** Selected momentum-distribution curves (MDCs) extracted from **a** (red), which were fitted to a function that adds two Lorentzian peaks and a linear background (black). **d** same as (**c**) for the spectral function shown in (**b**) with fits by single Lorentzian peaks. **e, g** Dispersion and FWHM extracted from fits to the ARPES MDCs. **f, h** Dispersion and FWHM extracted from MDC fits to the DMFT spectral function. The arrows in (**e, f, g,** and **h**) mark the position of two dispersion kinks.

parameters and assuming that the Fermi level is centered between the two lowest lying removal and addition states (see "methods" section for further details). Screening in a realistic lattice configuration is expected to decrease the energies of the transitions. The precise spectral weight distribution will be affected by additional effects that are not included in the atomic model, such as the specific d-orbital character, crystal field splittings, and hybridization with the As p-orbitals and resulting fluctuating valence state[49].

The comparison with the atomic model demonstrates that the observed three incoherent peaks in ARPES and DFT+DMFT represent the multiplet of Hubbard bands. The first high-spin Hubbard satellite (d^5, $S = \pm 5/2$) around −1 eV has previously been observed experimentally and theoretically in FeSe[45–49]. In addition, we expect a low-spin multiplet structure (d^5, $S = \pm 3/2$), which is located at higher energies due to the strong Hund's coupling effect. Arsenic p orbitals appear at a similar energy range (see Supplementary Note 1 Supplementary Material). Therefore, p-d hybridization is expected to alter the intensity distribution of the d_{xz} spectral function in this energy range. The extremely broad signatures in ARPES and DFT+DMFT between −2 eV and −4 eV in combination with the predictions from the atomic model demonstrate the existence of an additional low-spin multiplet structure (d^5, $S = \pm 3/2$) as would be expected for multiorbital systems[54].

The clear separation of coherent quasiparticle peak and incoherent Hubbard bands places RbFe$_2$As$_2$ into the realm of correlated materials that are predicted to show two kinks in the dispersion as described above.

A high-resolution ARPES spectrum across the energy scale of the expected kinks is presented in Fig. 2a. It clearly shows two dispersion kinks, which we verify by fitting of momentum distribution curves

(MDCs) as exemplified in Fig. 2c. The extracted dispersion in Fig. 2e demonstrates the strong renormalization at the two kink energies of 23 meV and 330 eV. The FWHM in Fig. 2g shows a step at each kink energy indicating a substantial increase in lifetime. Long-lived quasi-particles with a sharp spectral peak only develop at binding energies below the 23 meV kink. The flat dispersion in this energy range is consistent with the large effective mass from quantum oscillation measurements[32].

Typically, a self-energy is extracted from such an MDC analysis to compare with theoretical predictions. It requires the assumption of a bare-band dispersion, which would need to extend over more than 0.5 eV in our analysis and certainly involves a-priori unknown non-linear contributions. To circumvent this ambiguity, we instead perform the same MDC analysis on the spectral function obtained from our DFT+DMFT calculations as we did for the ARPES data. The corresponding spectrum with a selection of MDCs, as well as the extracted dispersion and FWHM are shown in Fig. 2b, d, f, and h respectively. The calculations reveal two kinks at almost the same energy scale and with very similar spectral appearance. The kinks represent the effect of the DMFT self-energy on the spectral function Supplementary Material. Hence, they do not originate from simple hybridization effects of different Fe 3d bands. A complimentary self-energy analysis of the ARPES data can be found in the Supplementary Note 3 Supplementary Material.

The high energy kink at 330 meV is well beyond the highest energy in the phonon spectrum[55] and it is therefore not due to electron-phonon coupling. The kink initiates a high-energy section of steep dispersion with reduced intensity, which connects the coherent quasiparticle component of the spectral function with the first incoherent Hubbard band that is centered around 1 eV binding energy. The experimental signatures are well reproduced by DMFT.

The kink can therefore be associated with the high-energy kink predicted by general theoretical models of strongly correlated systems[11]. The steep high-energy dispersion is reminiscent of the "waterfall" structure seen in cuprate superconductors[19–21], where it develops from the spectral signature of the Mott insulating state[29]. Unusual high-energy renormalizations have also been observed in other iron-based superconductors[45–47,56]. Among them are both parent and electron-doped compounds, which are much further away from a Mott transition and therefore less correlated than the hole-doped $RbFe_2As_2$. The same mechanism is likely responsible for these signatures and strong electronic correlations due to the interplay of Hubbard and Hund interactions, therefore, seem to play a crucial role for the vast majority of iron-based superconductors.

The kink energy of 23 meV lies within the phonon spectrum of $RbFe_2As_2$[55], which immediately suggests electron-phonon coupling as the origin. Such a kink is typically described with a Migdal-Eliashberg weak coupling mechanism. We can extract the corresponding coupling constant $\lambda = v_{highE}/v_{lowE} - 1 = 3$ from the change in dispersion. However, $\lambda = 3$ is much larger than the weak coupling limit. It is also considerably larger than 0.5 for kinks observed in various other FeSC[5–9]. Electron-phonon coupling from a standard weak-coupling mechanism is therefore unlikely to be responsible for the low-energy kink in $RbFe_2As_2$. A strong quasiparticle renormalization with an energy scale of approximately 20 meV was also observed in FeTe, which is one of the strongest correlated iron-chalcogenides. This has been interpreted as polaron formation due to the spectral lineshape

and the proximity of the kink to the phonon energy scale[57]. Another study suggested that spin-screening akin to Kondo coupling is responsible in line with an electronic origin[58].

The comparison to DFT+DMFT calculations sheds further light on the origin of the low-energy kink in $RbFe_2As_2$. Since the calculations do not include coupling to phonon excitations, all signatures are purely electronic in origin. The calculations show a similar kink at low energies. Apart from a difference in kink energy of approximately 35 meV, all other experimental signatures shown in Fig. 2 are very well reproduced by DMFT. In addition, the extracted Fermi velocities match almost perfectly (see Fig. 2e, f and Supplementary Note 5 for details Supplementary Material). These similarities suggest that the experimentally observed low-energy kink originates predominantly from electronic interactions.

Recent studies on FeSe demonstrated a cooperative enhancement of electron-electron and electron-phonon interactions and only taken together can they capture the experimental observations[59,60]. In particular, electronic correlations reduce the phonon mode frequencies in FeSe[61]. We speculate that such a cooperative mechanism influences the low-energy kink in $RbFe_2As_2$ and reduces the kink energy compared to the DMFT calculations.

Theoretical studies of the Hubbard, Kondo, and Hund-Hubbard model showed that the appearance of two kinks in correlated materials is related to a two-stage dynamics for establishing coherent quasiparticles[15,18]. It is therefore instructive to study the temperature dependence of the low-energy kink, which we show in Fig. 3. Note that

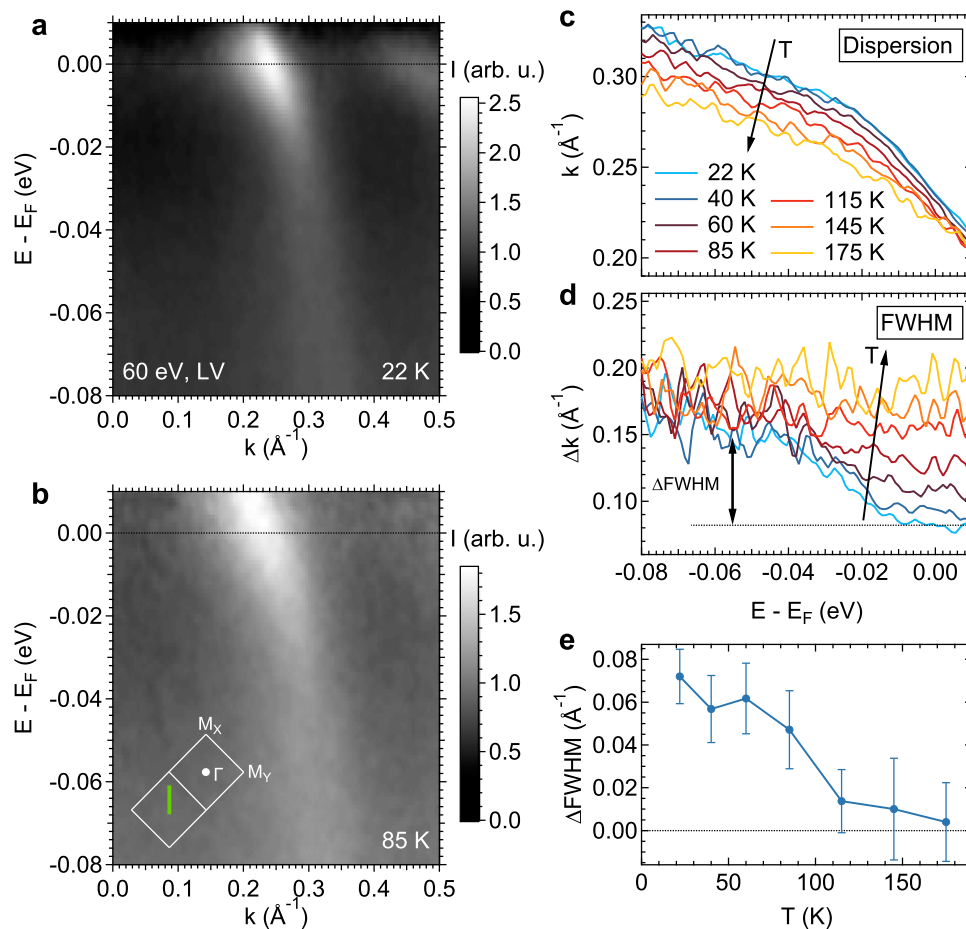**Fig. 3 | Temperature dependence of the low-energy kink. a, b** ARPES spectra taken at 22 K and 85 K, respectively. We used linearly vertically (LV) polarized light with an energy of 60 eV. The green line in the inset of (**b**) sketches the momentum cut through the Brillouin zones. The dot indicates normal emission geometry. **b, c** We obtain the dispersion and FWHM from an MDC analysis of ARPES spectra between 22 K and 175 K. **e** The step in the width $\Delta FWHM$ was determined from the difference in the average FWHM between (−70,−40) meV and (−10, 8) meV as sketched in (**d**). Error bars represent the standard deviation.

the data were taken along a different momentum cut than those in Fig. 2a. Both the kink in the dispersion and the step in the FWHM disappear at higher temperatures. To quantify the behavior, we calculate the difference of the average FWHM below and above the kink energy (ΔFWHM). Its temperature dependence shown in Fig. 3e indicates a crossover temperature around 70-100 K, which coincides very well with the spin-coherence scale of 90 K that was obtained from spin-susceptibility measurements[30]. Beyond this temperature, one expects a regime with damped quasiparticles, which agrees well with our experimentally observed increased width and decreased peak intensity. The analysis of the temperature dependence therefore supports our conclusion that the 23 meV kink is primarily electronic in origin. Very similar loss of renormalization and increased lifetime as a function of temperature was also observed with ARPES and DMFT in the Hund's metal Sr_2RuO_4[62].

A low-energy correlation-induced kink implies the existence of spin fluctuations with a peak in the spin susceptibility close to the kink energy[12,14,15,18]. It was suggested that the formation of the kink can be viewed as a coupling of electrons to these emergent internal bosonic modes[12]. One may speculate that such modes are also responsible for superconducting pairing. Unfortunately, neutron data are so far unavailable for $RbFe_2As_2$. However, recent measurements on the sister compound KFe_2As_2 showed clear evidence for spin excitations below 20 meV[63,64] that develop into a resonance inside the superconducting state[65]. KFe_2As_2 has the same doping and very similar electronic and superconducting properties that evolve smoothly across the chemical pressure series from KFe_2As_2 over $RbFe_2As_2$ to $CsFe_2As_2$[32–35,40]. Evidence for nodes in the superconducting gap function was found experimentally[31,66–73], but the superconducting pairing mechanism of these hole doped compounds is debated. Proposals range from spin-fluctuation mediated pairing[74–76], pairing due to strong Hund's electron-electron interaction[77], to pairing from orbital fluctuations[78]. Our discovery of a correlation-induced, strong low-energy kink on the same energy scale as spin fluctuations generates new perspectives for revealing the superconducting pairing mechanism in iron-based superconductors.

Methods

ARPES experiments

Single crystals of $RbFe_2As_2$ were grown from an FeAs flux[79]. ARPES measurements were performed at the SSRL synchrotron at beamline 5–2. Samples were glued onto copper sample holders and furnished with a ceramic top post using H20E epoxy. All gluing and curing steps were performed inside an argon glovebox. Samples were cleaved in-situ at a pressure of 3×10^{-11} torr and below 30 K. We oriented the samples along the in-plane high-symmetry crystallographic directions using Fermi surface measurements. We used a photon energy of 60 eV and linear vertically polarized light. The slit of the ARPES analyzer was vertically oriented. A sketch of the geometry and calculations of the photoemission matrix elements[80–82] can be found in the Supplementary Note 6 Supplementary Material. The samples are generally very soft and tend to buckle after cleaving. In order to obtain data from a pristine flat part of the sample surface, we used a small beam spot size of approximately $50\,\mu m$. The energy and angular resolution of the measurements is 16 and 0.1°, respectively. Data for Fig. 1 and 2 were obtained at 20 K across the center of the first Brillouin zone. Data for Fig. 3 were obtained in the second Brillouin zone at temperatures indicated in the figure. Additional supporting measurements have been performed at the MAESTRO beamline at the Advanced Light Source of the Lawrence Berkeley National Laboratory and at the Penn State Materials Research Institute.

DFT+DMFT calculations

For the fully charge self-consistent DFT+DMFT calculations we employ the implementation within the Wien2K package[83,84] of the full-potential linear augmented plane wave (FLAPW) method in the generalized gradient approximation[85], using a $17 \times 17 \times 17$ momentum grid discretization of the Brillouin zone. The Bloch wave functions were projected on the subspace of the correlated Fe 3d orbital[52,86], using a large window of [− 6, 13.6] eV, which includes the filled As p states and higher energy unoccupied states, resulting in 30 bands on average for each momentum state. The impurity model of the Fe 3d subspace was solved with the continuous-time quantum Monte Carlo method in the hybridization expansion, using the segment picture[87–89]. The calculations were done at a temperature of $T = 96K$, unless indicated otherwise. We used interaction parameters of $U_{avg} = 4eV$, $J_{avg} = 0.8$ eV, representative for the iron-based pnictides[53], in the definition of Slater integrals[90], and the nominal double counting correction[91,92] with $N = 5.5$ nominal filling. Real frequency data was obtained by performing stochastic analytical continuation[93] on the Matsubara self-energy, which was then used to calculate the momentum-resolved spectral function on real frequencies. Orbital occupations from DFT and DFT+DMFT, as well as projections of the spectral function onto other Fe 3d orbitals and the full spectral function summed over all states are presented in the Supplementary Note 2 Supplementary Material.

Atomic model

For the atomic model, we calculated the spectral function using the exact diagonalization of a degenerate five-orbital system with 6 electrons. We use the same interaction parameters U_{avg}, J_{avg} as for DMFT. The ground state is a high spin configuration d^6, $S = \pm 4/2$. Within this model we can identify the following possible atomic multiplets: 3 electron removal states, which correspond to the three possible choices of removing an electron either from the doubly occupied orbital to result in a d^5, $S = \pm 5/2$, or $S = \pm 3/2$ configuration. Or, removing an electron from one of the single occupied orbitals, resulting in a $S = \pm 3/2$ configuration. There is only one possible electron addition state, resulting in d^7, $S = \pm 3/2$. Their removal (addition) state energies are at $(U - 3J)/2$ eV, $(U + 5J)/2$, and $(U + 9J)/2$ eV $(- (U - 3J)/2$ eV), assuming that the Fermi level is centered between the two lowest lying removal and addition states.

Data availability

The datasets generated during the current study are available from the corresponding authors upon request.

Code availability

The custom codes implementing the calculations of this study are available from the corresponding authors upon request.

References

1. Damascelli, A., Hussain, Z. & Shen, Z.-X. Angle-resolved photoemission studies of the cuprate superconductors. *Rev. Mod. Phys.* **75**, 473–541 (2003).
2. Sobota, J. A., He, Y. & Shen, Z.-X. Angle-resolved photoemission studies of quantum materials. *Rev. Mod. Phys.* **93**, 025006 (2021).
3. Iwasawa, H. et al. High-energy anomaly in the band dispersion of the ruthenate superconductor. *Phys. Rev. Lett.* **109**, 066404 (2012).
4. Tamai, A. et al. High-resolution photoemission on Sr_2RuO_4 reveals correlation-enhanced effective spin-orbit coupling and dominantly local self-energies. *Phys. Rev. X* **9**, 021048 (2019).
5. Wray, L. et al. Momentum dependence of superconducting gap, strong-coupling dispersion kink, and tightly bound cooper pairs in the high-T_c (Sr, Ba)$_{1-x}$(K, Na)$_x$Fe$_2$As$_2$ superconductors. *Phys. Rev. B* **78**, 184508 (2008).
6. Koitzsch, A. et al. Temperature and doping-dependent renormalization effects of the low energy electronic structure of Ba$_{1-x}$K$_x$Fe$_2$As$_2$ single crystals. *Phys. Rev. Lett.* **102**, 167001 (2009).
7. Richard, P. et al. Angle-resolved photoemission spectroscopy of the Fe-based Ba$_{0.6}$K$_{0.4}$Fe$_2$As$_2$ high temperature superconductor:

evidence for an orbital selective electron-mode coupling. *Phys. Rev. Lett.* **102**, 47003 (2009).

8. Kordyuk, A. A. et al. Angle-resolved photoemission spectroscopy of superconducting LiFeAs: evidence for strong electron-phonon coupling. *Phys. Rev. B* **83**, 134513 (2011).

9. Malaeb, W. et al. Evidence of a universal relation between electron-mode coupling and T_c in Ba$_{1-x}$K$_x$Fe$_2$As$_2$ superconductor from laser angle-resolved photoemission spectroscopy. *Phys. Rev. B* **90**, 195124 (2014).

10. Jang, B. G. et al. Direct observation of kink evolution due to Hund's coupling on approach to metal-insulator transition in NiS$_{2-x}$Se$_x$. *Nat. Commun.* **12**, 1208 (2021).

11. Byczuk, K. et al. Kinks in the dispersion of strongly correlated electrons. *Nat. Phys.* **3**, 168–171 (2007).

12. Raas, C., Grete, P. & Uhrig, G. S. Emergent collective modes and kinks in electronic dispersions. *Phys. Rev. Lett.* **102**, 76406 (2009).

13. Deng, X. et al. How bad metals turn good: spectroscopic signatures of resilient quasiparticles. *Phys. Rev. Lett.* **110**, 86401 (2013).

14. Held, K., Peters, R. & Toschi, A. Poor man's understanding of kinks originating from strong electronic correlations. *Phys. Rev. Lett.* **110**, 246402 (2013).

15. Stadler, K. M., Kotliar, G., Lee, S.-S. B., Weichselbaum, A. & von Delft, J. Differentiating hund from mott physics in a three-band Hubbard-hund model: temperature dependence of spectral, transport, and thermodynamic properties. *Phys. Rev. B* **104**, 115107 (2021).

16. Matsuyama, K., Perepelitsky, E. & Shastry, B. S. Origin of kinks in the energy dispersion of strongly correlated matter. *Phys. Rev. B* **95**, 165435 (2017).

17. Kugler, F. B., Lee, S.-S. B., Weichselbaum, A., Kotliar, G. & von Delft, J. Orbital differentiation in hund metals. *Phys. Rev. B* **100**, 115159 (2019).

18. Hu, D., Tong, N.-H. & Yang, Y.-f Energy-scale cascade and correspondence between Mott and Kondo lattice physics. *Phys. Rev. Res.* **2**, 43407 (2020).

19. Ronning, F. et al. Anomalous high-energy dispersion in angle-resolved photoemission spectra from the insulating cuprate Ca$_2$CuO$_2$Cl$_2$. *Phys. Rev. B* **71**, 094518 (2005).

20. Meevasana, W. et al. Hierarchy of multiple many-body interaction scales in high-temperature superconductors. *Phys. Rev. B* **75**, 174506 (2007).

21. Xie, B. P. et al. High-energy scale revival and giant kink in the dispersion of a cuprate superconductor. *Phys. Rev. Lett.* **98**, 147001 (2007).

22. Valla, T. et al. High-energy kink observed in the electron dispersion of high-temperature cuprate superconductors. *Phys. Rev. Lett.* **98**, 167003 (2007).

23. Graf, J. et al. Universal high energy anomaly in the angle-resolved photoemission spectra of high temperature superconductors: Possible evidence of spinon and holon branches. *Phys. Rev. Lett.* **98**, 067004 (2007).

24. Meevasana, W. et al. Extracting the spectral function of the cuprates by a full two-dimensional analysis: angle-resolved photoemission spectra of Bi$_2$Sr$_2$CuO$_6$. *Phys. Rev. B* **77**, 104506 (2008).

25. Macridin, A., Jarrell, M., Maier, T. & Scalapino, D. J. High-energy kink in the single-particle spectra of the two-dimensional Hubbard model. *Phys. Rev. Lett.* **99**, 237001 (2007).

26. Moritz, B. et al. Effect of strong correlations on the high energy anomaly in hole- and electron-doped high-tc superconductors. *N. J. Phys.* **11**, 093020 (2009).

27. Moritz, B., Johnston, S. & Devereaux, T. P. Insights on the cuprate high energy anomaly observed in ARPES. *J. Electron Spectrosc. Relat. Phenom.* **181**, 31–34 (2010).

28. Kim, M., Mravlje, J., Ferrero, M., Parcollet, O. & Georges, A. Spin-orbit coupling and electronic correlations in Sr$_2$RuO$_4$. *Phys. Rev. Lett.* **120**, 126401 (2018).

29. Wang, Y. et al. Emergence of quasiparticles in a doped mott insulator. *Commun. Phys.* **3**, 210 (2020).

30. Khim, S. et al. A calorimetric investigation of RbFe$_2$As$_2$ single crystals. *Phys. status solidi (b)* **254**, 1600208 (2017).

31. Zhang, Z. et al. Heat transport in RbFe$_2$As$_2$ single crystals: evidence for nodal superconducting gap. *Phys. Rev. B* **91**, 024502 (2015).

32. Eilers, F. et al. Strain-driven approach to quantum criticality in AFe$_2$As$_2$ with A = K, Rb, and Cs. *Phys. Rev. Lett.* **116**, 237003 (2016).

33. Xiang, Z. J. et al. Incoherence-coherence crossover and low-temperature fermi-liquid-like behavior in AFe$_2$As$_2$ (A=K, Rb, Cs): evidence from electrical transport properties. *J. Phys.: Condens. Matter* **28**, 425702 (2016).

34. Wu, Y. P. et al. Emergent kondo lattice behavior in iron-based superconductors AFe$_2$As$_2$ (A=K, Rb, Cs). *Phys. Rev. Lett.* **116**, 147001 (2016).

35. Wiecki, P. et al. Emerging symmetric strain response and weakening nematic fluctuations in strongly hole-doped iron-based superconductors. *Nat. Commun.* **12**, 4824 (2021).

36. Haule, K. & Kotliar, G. Coherence-incoherence crossover in the normal state of iron oxypnictides and importance of Hund's rule coupling. *N. J. Phys.* **11**, 25021 (2009).

37. De' Medici, L. Hund's coupling and its key role in tuning multiorbital correlations. *Phys. Rev. B* **83**, 205112 (2011).

38. De' Medici, L., Mravlje, J. & Georges, A. Janus-faced influence of Hund's rule coupling in strongly correlated materials. *Phys. Rev. Lett.* **107**, 256401 (2011).

39. De' Medici, L., Giovannetti, G. & Capone, M. Selective mott physics as a key to iron superconductors. *Phys. Rev. Lett.* **112**, 177001 (2014).

40. Backes, S., Jeschke, H. O. & Valentí, R. Microscopic nature of correlations in multiorbital AFe$_2$As$_2$ (A=K, Rb, Cs): Hund's coupling versus coulomb repulsion. *Phys. Rev. B* **92**, 195128 (2015).

41. Stadler, K., Kotliar, G., Weichselbaum, A. & von Delft, J. Hundness versus mottness in a three-band Hubbard-hund model: on the origin of strong correlations in hund metals. *Ann. Phys.* **405**, 365–409 (2019).

42. Yi, M., Zhang, Y., Shen, Z.-X. & Lu, D. Role of the orbital degree of freedom in iron-based superconductors. *npj Quantum Mater.* **2**, 57 (2017).

43. Kong, S. et al. Electronic structure in a one-Fe Brillouin zone of the iron pnictide superconductors CsFe$_2$As$_2$ and RbFe$_2$As$_2$. *Phys. Rev. B* **92**, 184512 (2015).

44. Yeh, J. & Lindau, I. Atomic subshell photoionization cross sections and asymmetry parameters: $1 \leqslant z \leqslant 103$. *Data Nucl. Data Tables* **32**, 1–155 (1985).

45. Evtushinsky, D. V. et al. Direct observation of dispersive lower Hubbard band in iron-based superconductor FeSe. *Preprint* https://doi.org/10.48550/arXiv.1612.02313 (2016).

46. Watson, M. D. et al. Formation of Hubbard-like bands as a fingerprint of strong electron-electron interactions in FeSe. *Phys. Rev. B* **95**, 81106 (2017).

47. Pfau, H. et al. Quasiparticle coherence in the nematic state of FeSe. *Phys. Rev. B* **104**, L241101 (2021).

48. Aichhorn, M., Biermann, S., Miyake, T., Georges, A. & Imada, M. Theoretical evidence for strong correlations and incoherent metallic state in fese. *Phys. Rev. B* **82**, 064504 (2010).

49. Yin, Z., Haule, K. & Kotliar, G. Kinetic frustration and the nature of the magnetic and paramagnetic states in iron pnictides and iron chalcogenides. *Nat. Mater.* **10**, 932–935 (2011).

50. Ferber, J., Foyevtsova, K., Valentí, R. & Jeschke, H. O. Lda+ dmft study of the effects of correlation in LiFeAs. *Phys. Rev. B* **85**, 094505 (2012).

51. Ferber, J., Jeschke, H. O. & Valentí, R. Fermi surface topology of lafepo and lifep. *Phys. Rev. Lett.* **109**, 236403 (2012).

52. Aichhorn, M. et al. Dynamical mean-field theory within an augmented plane-wave framework: assessing electronic correlations in the iron pnictide LaFeAsO. *Phys. Rev. B* **80**, 085101 (2009).

53. van Roekeghem, A., Vaugier, L., Jiang, H. & Biermann, S. Hubbard interactions in iron-based pnictides and chalcogenides: slater parametrization, screening channels, and frequency dependence. *Phys. Rev. B* **94**, 125147 (2016).

54. Środa, M., Mravlje, J., Alvarez, G., Dagotto, E. & Herbrych, J. Hund bands in spectra of multiorbital systems. *Phys. Rev. B* **108**, L081102 (2023).

55. Richard, P. et al. Van Hove singularities, chemical pressure and phonons: an angle-resolved photoemission study of kfe $_2$as $_2$ and csfe $_2$as $_2$. *arXiv preprint* https://doi.org/10.48550/arXiv.1807.00193 (2018).

56. Evtushinsky, D. V. et al. High-energy electronic interaction in the 3d band of high-temperature iron-based superconductors. *Phys. Rev. B* **96**, 060501 (2017).

57. Liu, Z. K. et al. Measurement of coherent polarons in the strongly coupled antiferromagnetically ordered iron-chalcogenide $Fe_{1.02}Te$ using angle-resolved photoemission spectroscopy. *Phys. Rev. Lett.* **110**, 037003 (2013).

58. Kim, Y. et al. Kondo interaction in fete and its potential role in the magnetic order. *Nat. Commun.* **14**, 4145 (2023).

59. Mandal, S., Cohen, R. E. & Haule, K. Strong pressure-dependent electron-phonon coupling in FeSe. *Phys. Rev. B* **89**, 220502 (2014).

60. Gerber, S. et al. Femtosecond electron-phonon lock-in by photoemission and x-ray free-electron laser. *Science* **357**, 71–75 (2017).

61. Khanal, G. & Haule, K. Correlation driven phonon anomalies in bulk fese. *Phys. Rev. B* **102**, 241108 (2020).

62. Hunter, A. et al. Fate of quasiparticles at high temperature in the correlated metal Sr_2RuO_4. *Phys. Rev. Lett.* **131**, 236502 (2023).

63. Lee, C. H. et al. Incommensurate spin fluctuations in hole-overdoped superconductor KFe_2As_2. *Phys. Rev. Lett.* **106**, 67003 (2011).

64. Wang, M. et al. Doping dependence of spin excitations and its correlations with high-temperature superconductivity in iron pnictides. *Nat. Commun.* **4**, 2874 (2013).

65. Shen, S. et al. Neutron spin resonance in the heavily hole-doped KFe_2As_2 superconductor. *Phys. Rev. Lett.* **124**, 017001 (2020).

66. Liu, X. et al. Evidence of nematic order and nodal superconducting gap along [110] direction in $RbFe_2As_2$. *Nat. Commun.* **10**, 1039 (2019).

67. Okazaki, K. et al. Octet-line node structure of superconducting order parameter in KFe_2As_2. *Science* **337**, 1314–1317 (2012).

68. Hashimoto, K. et al. Evidence for superconducting gap nodes in the zone-centered hole bands of KFe_2As_2 from magnetic penetration-depth measurements. *Phys. Rev. B* **82**, 014526 (2010).

69. Kim, H. et al. Evolution of london penetration depth with scattering in single crystals of $K_{1-x}Na_xFe_2As_2$. *Phys. Rev. B* **89**, 174519 (2014).

70. Cho, K. et al. Energy gap evolution across the superconductivity dome in single crystals of $(Ba_{1-x}K_x)Fe_2As_2$. *Sci. Adv.* **2**, e1600807 (2016).

71. Reid, J.-P. et al. Universal heat conduction in the iron arsenide superconductor KFe_2As_2: evidence of a d-wave state. *Phys. Rev. Lett.* **109**, 087001 (2012).

72. Dong, J. K. et al. Quantum criticality and nodal superconductivity in the feas-based superconductor KFe_2As_2. *Phys. Rev. Lett.* **104**, 087005 (2010).

73. Watanabe, D. et al. Doping evolution of the quasiparticle excitations in heavily hole-doped $Ba_{1-x}K_xFe_2As_2$: A possible superconducting gap with sign-reversal between hole pockets. *Phys. Rev. B* **89**, 115112 (2014).

74. Suzuki, K., Usui, H. & Kuroki, K. Spin fluctuations and unconventional pairing in KFe_2As_2. *Phys. Rev. B* **84**, 144514 (2011).

75. Maiti, S., Korshunov, M. M., Maier, T. A., Hirschfeld, P. J. & Chubukov, A. V. Evolution of the superconducting state of Fe-based compounds with doping. *Phys. Rev. Lett.* **107**, 147002 (2011).

76. Thomale, R., Platt, C., Hanke, W., Hu, J. & Bernevig, B. A. Exotic d-wave superconducting state of strongly hole-doped $K_xBa_{1-x}Fe_2As_2$. *Phys. Rev. Lett.* **107**, 117001 (2011).

77. Vafek, O. & Chubukov, A. V. Hund interaction, spin-orbit coupling, and the mechanism of superconductivity in strongly hole-doped iron pnictides. *Phys. Rev. Lett.* **118**, 087003 (2017).

78. Kontani, H. & Onari, S. Orbital-fluctuation-mediated superconductivity in iron pnictides: analysis of the five-orbital hubbard-holstein model. *Phys. Rev. Lett.* **104**, 157001 (2010).

79. Chu, J.-H., Analytis, J. G., Kucharczyk, C. & Fisher, I. R. Determination of the phase diagram of the electron-doped superconductor $Ba(Fe_{1-x}Co_x)_2as_2$. *Phys. Rev. B* **79**, 014506 (2009).

80. Goldberg, S., Fadley, C. & Kono, S. Photoelectric cross-sections for fixed-orientation atomic orbitals: relationship to the plane-wave final state approximation and angle-resolved photoemission. *Solid State Commun.* **28**, 459 – 463 (1978).

81. Gadzuk, J. W. Angle-resolved photoemission from crystal-field split d shells of adsorbed atoms. *Phys. Rev. B* **12**, 5608–5614 (1975).

82. Li, Y.-F. et al. Orbital ingredients and persistent Dirac surface state for the topological band structure in $FeTe_{0.55}Se_{0.45}$. *Phys. Rev. X* **14**, 021043 (2024).

83. Blaha, P. et al. *WIEN2k, An Augmented Plane Wave + Local Orbitals Program for Calculating Crystal Properties*. (Karlheinz Schwarz, Techn. Universität Wien, Austria), (2018).

84. Blaha, P. et al. WIEN2k: An APW+lo program for calculating the properties of solids. *J. Chem. Phys.* **152**, 074101 (2020).

85. Perdew, J. P., Burke, K. & Ernzerhof, M. Generalized gradient approximation made simple. *Phys. Rev. Lett.* **77**, 3865–3868 (1996).

86. Ferber, J., Foyevtsova, K., Jeschke, H. O. & Valentí, R. Unveiling the microscopic nature of correlated organic conductors: The case of κ-$(ET)_2Cu[N(CN)_2]Br_xCl_{1-x}$. *Phys. Rev. B* **89**, 205106 (2014).

87. Werner, P., Comanac, A., de' Medici, L., Troyer, M. & Millis, A. J. Continuous-time solver for quantum impurity models. *Phys. Rev. Lett.* **97**, 076405 (2006).

88. Wallerberger, M. et al. Updated core libraries of the Alps project. *Preprint* on https://doi.org/10.48550/arXiv.1811.08331 (2018).

89. Bauer, B. et al. The Alps project release 2.0: open source software for strongly correlated systems. *J. Stat. Mech.: Theory Exp.* **2011**, P05001 (2011).

90. Liechtenstein, A. I., Anisimov, V. I. & Zaanen, J. Density-functional theory and strong interactions: orbital ordering in mott-hubbard insulators. *Phys. Rev. B* **52**, R5467–R5470 (1995).

91. Haule, K., Birol, T. & Kotliar, G. Covalency in transition-metal oxides within all-electron dynamical mean-field theory. *Phys. Rev. B* **90**, 075136 (2014).

92. Haule, K. Exact double counting in combining the dynamical mean field theory and the density functional theory. *Phys. Rev. Lett.* **115**, 196403 (2015).

93. Beach, K. S. D. et al. Identifying the maximum entropy method as a special limit of stochastic analytic continuation. https://doi.org/10.48550/arXiv.cond-mat/0403055 (2004).

Acknowledgements

Author contributions

H.P. conceived the experiment. G.-Y.C. and H.-H.W. synthesized the bulk single crystals. H.P., N.G., and D.L. performed the ARPES measurements with assistance from M.H. M.-H.C. performed the ARPES data analysis with assistance from H.P. R.V., S.B., and H.P. conceived the theoretical analysis. S.B. performed the DFT+DMFT calculations and those for the atomic model. S.B., D.L., M.H., S.-K.M., R.V., and H.P. interpreted the results of this study. H.P., S.B., and R.V. wrote the manuscript with input from all authors.

Competing interests

The authors declare no competing interests.

Additional information

Supplementary information The online version contains supplementary material available at https://doi.org/10.1038/s41467-024-54330-x.

Correspondence and requests for materials should be addressed to R. Valentí or H. Pfau.

Peer review information *Nature Communications* thanks Ji Hoon Shim, Rui Lou and the other, anonymous, reviewers for their contribution to the peer review of this work. A peer review file is available.

Reprints and permissions information is available at http://www.nature.com/reprints

Publisher's note Springer Nature remains neutral with regard to jurisdictional claims in published maps and institutional affiliations.